

Polymer-MOF Hybrid Composites with High Porosity and Stability through Surface-Selective Ligand Exchange

Vincent J. Pastore, Timothy R. Cook*, Javid Rzayev*

Department of Chemistry, University at Buffalo, the State University of New York, Buffalo, New York 14260-3000, United States

ABSTRACT: Hybrid materials containing organic polymers and metal-organic frameworks (MOFs) have attracted attention for their potential to harness both diverse functionality and high processability, but their fabrication is challenged by incompatibilities of the parent components. The poor solubility of MOFs hinders uniform dispersion throughout a polymer matrix, and may cause aggregation that is not only detrimental to the permeability of substrates, but also limits the structural integrity of the polymer. Meanwhile, polymer chains can block or penetrate the porous structures and compromise MOF functionality by reducing surface area and pore-size. We report a versatile method of covalent hybridization through post-synthetic ligand exchange to form a crosslinked polymer-MOF composite. The resulting network structure allows for the formation of robust, monolithic composites with variable MOF loadings that may exceed 80% wherein ligand exchange is limited to surface sites so as to fully preserve MOF surface area and porosity. The synthesis can be performed from a diverse set of inexpensive starting materials, encouraging the design of new functional materials across a wide range of applications.

INTRODUCTION

In the last two decades, MOFs have become a major focus of materials research.¹⁻⁴ Their angstrom-scale order, high porosity, functional tunability, and facile synthetic methods make them well suited for a wide range of applications.⁵⁻¹⁰ These attractive features are tempered by the poor physical strength and low processability of MOFs.¹¹ The crystalline frameworks are brittle and typically exist as insoluble powders. Additionally, many of the most commonly researched MOFs are hydrolytically unstable, suffering from irreversible structural degradation after a few hours of exposure to humid air.¹²⁻¹⁴

Recently, there have been several efforts to improve the physical properties of metal-organic frameworks by direct covalent integration with amorphous, organic polymers (Figure 1).¹⁵ These materials force uniform polymer-MOF integration and improve bulk physical strength; the polymer chains help to support the framework structure and increase stability. Such integration has most commonly been achieved by post-synthetic polymerization from initiator-functionalized ligands,^{11, 16-17} post-synthetic coupling of end-capped polymers to functionalized ligands¹⁸⁻¹⁹, or pre-synthetic ligand polymerization.²⁰⁻²¹ Wang and coworkers functionalized the benzene dicarboxylate (BDC) linkers of a $Zr_6O_4(OH)_4(BDC-NH_2)$ MOF (UiO-66-NH₂) with a methacrylamide initiating group.¹⁶ The MOF was then suspended in a solution of methacrylate monomer, and the polymer was grown directly from the ligands by UV-induced polymerization. This approach was used to produce freestanding hybrid membranes; however, it was not selective to the outer surface of the crystals, resulting in polymerization

throughout the pore volume. As a result, initiator functionalization alone decreased the BET surface of the crystals significantly.

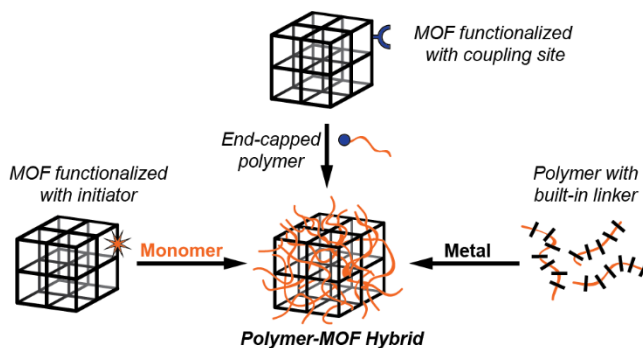


Figure 1. Previous methods of direct polymer-MOF integration through functionalized ligands to synthesize a hybrid crystal with polymer chains throughout the pores.

To blend MOFs and polymers selectively at the crystal surface, Kokado and Sada et. al. submerged UiO-66-NH₂ crystals in a solution of poly(*N*-isopropylacrylamide) (PNIPAM) end-capped with *N*-hydroxysuccinimide (NHS) and heated at 60°C.¹⁸ Because the polymer molecules were larger than the framework pore aperture, coupling was limited to exposed surface ligands and the bulk porosity was preserved. The resulting UiO-66-PNIPAM hybrid particles demonstrated controlled host-guest behavior, though they existed as individual nanoparticles rather than membranes.

More recently, it has been discovered by Cohen et. al. that ligands incorporated into a polymer backbone will assemble with

the proper metal precursors to form a framework structure, resulting in “polyMOFs,” wherein every ligand is connected through a polymer chain.²⁰ These polyMOFs demonstrate improved water stability, with no structural deformation observed until after 3 days of exposure to ambient air. By using tailor-made polymers with precisely spaced ligand fragments, Cohen et al. were able to fabricate polyMOFs with surface areas ranging from 70 to 1104 m²g⁻¹, which are remarkably high for a polymeric material. In this approach, the polymer segments connecting ligand moieties become part of the crystal and cause inevitable decrease in surface area compared to the parent MOF (2963 m²g⁻¹). In order to maximize the functionality of the original MOF, in this work we focused on developing a scalable method of integration based on covalent attachment of polymer chains to a MOF surface, while leaving the majority of the crystal structure and porosity undisturbed.

Polyimides have been studied extensively for applications in membrane technology, including mixed matrix membranes, due to their high mechanical strength, chemical resistance, and thermal stability resulting from rigid aromatic backbones and strong intermolecular forces.²²⁻²⁴ They are synthesized using a simple and inexpensive two-step method, beginning with a polycondensation between dianhydride and diamine monomers in air at room temperature to form a soluble poly(amic acid). This intermediate is then converted to the insoluble polyimide product through a thermal cyclization at 150-300°C post processing. One such polyimide, poly(4,4'-oxydiphenylene-pyromellitimide), was developed by researchers at DuPont in the 1960s and has since become an industry standard in applications from x-ray windows to spacecraft.²⁵ With a glass transition temperature (T_g) above 350°C, a tensile strength over 200 MPa, and a decomposition temperature above 500°C, this polyimide exhibits remarkable physical properties for a plastic.²⁶ However, it has attracted our attention not only for its strength, but for the chemical structure of the poly(amic acid) intermediate.

Synthesized from 4-aminophenyl ether and 1,2,4,5-benzenetetracarboxylic anhydride monomers, approximately half of the repeat units feature the *para*-substituted benzene dicarboxylate (BDC) moiety built into the polymer backbone, with the other half containing the *meta*-substituted BDC from the nonselective ring opening (Figure 2). The *para*-BDC group is commonly used as a linker in MOF structures, meaning the polymer is not only an incredible thermoplastic, but also a strong candidate for a new method of hybridization.

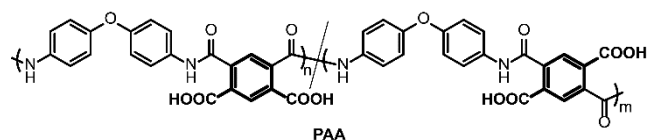


Figure 2. Structure of a poly(amic acid) intermediate, poly(pyromellitic dianhydride-co-4,4'-oxydianiline), featuring the BDC moiety (bold) within the polymer backbone.

In this work, we report a versatile polymer-MOF hybridization using ligand exchange between pure MOF crystals and ligand moieties incorporated into a poly(amic acid) backbone (Figure 3). Post-synthetic ligand exchange occurs heterogeneously when a MOF is suspended in a solution of alternate ligands.²⁷⁻²⁸ This exchange process is reversible and only requires mild reaction conditions when labile metal-ligand bonds are present. Studies have shown post-synthetic ligand exchange, pioneered

by Cohen et al., to be an effective strategy for MOF functionalization using a variety of metal-ligand combinations,²⁹ but to the best of our knowledge it has not previously been applied to polymeric ligands. Herein, we disclose a method in which post-synthetic ligand exchange is used to covalently integrate poly(amic acid) and MOF structures through the BDC moieties in the polymer backbone. The product of this integration is a crosslinked composite in which each junction is a MOF, allowing for improvements in strength, flexibility, and stability while retaining the porosity of the pure framework. We demonstrate that this technique can be used to synthesize polymer-MOF hybrid materials from a variety of components, creating a pathway for further evolution of functional materials.

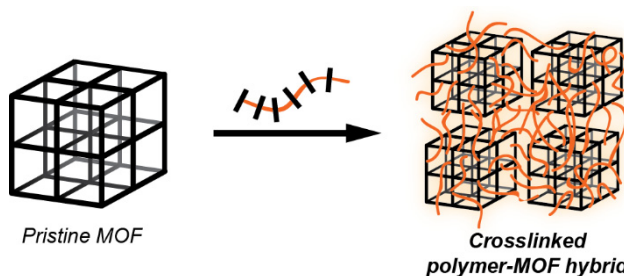


Figure 3. Schematic of direct integration through postsynthetic ligand exchange to form a crosslinked polymer-MOF network with preserved porosity.

EXPERIMENTAL

Materials. 4-aminophenyl ether (ODA), 2-methylimidazole (2-MIM), 1,2,4,5-benzenetetracarboxylic anhydride (PMDA), and pyridine were purchased from Acros Organics. Zirconium tetrachloride and triphenylphosphine were purchased from Alfa Aesar. Zinc nitrate hexahydrate ($Zn(NO_3)_2 \cdot 6H_2O$) was purchased from Aqua Solutions, Inc. Aniline was purchased from Beantown Chemical. Triethylamine (TEA) was purchased from EMD Millipore. Acetone, ethanol, and methanol were purchased from Fisher Scientific. N,N-dimethylformamide (DMF) was purchased from Macron Fine Chemicals. Oxalyl chloride (2.0 M in CH_2Cl_2), 4-vinylbenzoic acid (4-VBA), hexachloroethane, N-methyl-2-pyrrolidone (NMP) and azobisisobutyronitrile (AIBN) were purchased from Sigma-Aldrich. Terephthalic acid (H_2BDC) was purchased from TCI chemicals. 4-VBA was recrystallized from 30% ethanol in water, and AIBN was recrystallized from methanol. All other chemicals were used as received without further purification.

MOF Synthesis. All MOFs were synthesized based on previously published procedures. The synthesized materials were dried in a vacuum oven at 100°C for 24 hours and stored in a desiccator (Drierite) until use. Structures were confirmed by PXRD using simulated patterns from previously reported measurements as reference (Figures S1-S3).

MOF-5 microcrystals.^{11, 30-31} A solution of H_2BDC (2.0 g, 12 mmol) in DMF (100 mL) was added to a solution of $Zn(NO_3)_2 \cdot 6H_2O$ (10.8 g, 36.3 mmol) in DMF (200 mL) in a 1-L round bottom flask and set to stir at 120°C for 48 hours. The reaction was cooled to room temperature and colorless crystals were collected by vacuum filtration and washed with DMF followed by acetone.

MOF-5 nanocrystals.³² TEA (2.2 mL, 1.6 g, 16 mmol) was added to a solution of $Zn(NO_3)_2 \cdot 6H_2O$ (1.21 g, 4.07 mmol) and H_2BDC (0.34 g, 2.0 mmol) in DMF (40 mL) over 5 minutes

with vigorous stirring. The solution was set to stir at room temperature for 3 hours, after which the white precipitate was collected by centrifugation and washed with DMF followed by acetone.

ZIF-8.³³ A solution of 2-MIM (668 mg, 8.13 mmol) in DMF (40 mL) was added to a solution of $\text{Zn}(\text{NO}_3)_2 \cdot 6\text{H}_2\text{O}$ (2.68 g, 9.01 mmol) in DMF (160 mL) in a 500-mL round bottom flask and heated to 140°C under static conditions for 24 hours. The reaction was removed from heat and cooled to room temperature and pale yellow crystals were collected by vacuum filtration and washed with DMF followed by acetone.

UiO-66.³⁴ Concentrated HCl (4 mL) was added to a solution of ZrCl_4 (500 mg, 2 mmol) in DMF (20 mL) in a 200-mL round bottom flask. A solution of H_2BDC (500 mg, 3 mmol) in DMF (40 mL) was added and the solution was heated to 80°C under static conditions for 24 hours. The reaction was cooled to room temperature and the colorless crystals were collected by vacuum filtration and washed with DMF followed by acetone.

Polymer Synthesis. All polymers were synthesized following previously reported procedures.

Poly(pyromellitic dianhydride-co-4,4'-oxydianiline) (PAA).^{26, 35-36} A solution of ODA (2.80 g, 14.0 mmol) in DMF (10 mL) was added to a solution of PMDA (3.05 g, 14.0 mmol) in DMF (30 mL) and set to stir at room temperature for 24 hours. The polymer was precipitated into methanol/brine and washed with excess water to remove DMF. The light yellow polymer was collected by centrifugation and dried overnight in a vacuum oven at room temperature. $^1\text{H NMR}$ ($(\text{CD}_3)_2\text{SO}$, 25°C): δ (ppm) = 13.32 (4H, br), 10.57 (4H, br), 8.31 (1H, br), 7.97 (2H, br), 7.73 (1H, br), 7.70 (8H, br), 7.03 (8H, br). ATR-FTIR: ν_{max} / cm^{-1} = 2981 (br), 1714, 1640, 1537, 1495, 1409, 1383, 1212, 1100, 1013, 872, 829, 757, 661. For synthesis of PAA at low molecular weights, the same procedure was used as above, but with the addition of a 0.2 molar equivalence of aniline to the reaction solution.

Poly(dicarbomethoxyterephthalic acid-co-4,4'-oxydianiline) (MEPA).³⁷⁻³⁸ PMDA (2.0 g, 9.2 mmol) was dissolved in anhydrous methanol (20 mL) and set to reflux under N_2 for 5 hours. The solution was allowed to cool to room temperature and solvent was removed under reduced pressure to give a mixture of *meta*- and *para*-pyromellitic acid dimethyl ester (PMDE) as a white solid (2.6 g, 9.2 mmol, quantitative yield). $^1\text{H NMR}$ ($(\text{CD}_3)_2\text{SO}$, 25°C): δ (ppm) = 13.82 (4H, s), 8.10 (1H, s), 8.01 (2H, s), 7.93 (1H, s), 3.84 (12H, s). PMDE (250 mg, 0.89 mmol), ODA (177 mg, 0.883 mmol), and PPh_3 (558 mg, 2.13 mmol) were dissolved in a mixture of pyridine (1.5 mL) and NMP (4.4 mL). Hexachloroethane (630 mg, 2.7 mmol) was added and the solution was set to stir at room temperature for 24 hours. The yellow-orange polymer was precipitated into 0.5 M HCl in H_2O followed by pure H_2O , collected by centrifugation, and dried overnight in a vacuum oven at room temperature. $^1\text{H NMR}$ ($(\text{CD}_3)_2\text{SO}$, 25°C): δ (ppm) = 10.60 (4H, br), 8.29 (1H, br), 8.06 (2H, br), 7.90 (1H, br), 7.70 (8H, br), 7.05 (8H, br), 3.83 (12H, br). ATR-FTIR: ν_{max} / cm^{-1} = 3255 (br), 1725, 1651, 1607, 1540, 1497, 1436, 1409, 1299, 1239, 1215, 1167, 1101, 1013, 965, 872, 831, 779, 722, 695, 540, 517.

Poly(4-vinylbenzoic acid) (PVBA).³⁹⁻⁴⁰ A degassed solution of 4-VBA (175 mg, 1.18 mmol) and AIBN (1.9 mg, 0.012 mmol) in DMF (1 mL) was stirred at 70°C under N_2 . The reaction was cooled to room temperature and precipitated into water. The

white polymer was collected by centrifugation and dried overnight in a vacuum oven at room temperature. $^1\text{H NMR}$ ($(\text{CD}_3)_2\text{SO}$, 25°C): δ (ppm) = 7.87-7.36 (2H, br), 6.82-6.30 (2H, br), 2.14-1.11 (3H, br). ATR-FTIR: ν_{max} / cm^{-1} = 2925 (br), 2655 (br), 1682, 1607, 1509, 1419, 1385, 1280, 1178, 1104, 1017, 920, 857, 777, 706, 671, 543.

Polymer-MOF composite synthesis. Hybrid materials were synthesized using the following procedures. All synthesized materials were dried under atmospheric conditions and stored in a desiccator (Drierite) until further use.

Dynamic synthesis. Materials containing 20, 40, 60 and 80% (w/w) MOF-5 were synthesized using MOF/polymer weight ratios of 40/160 mg, 80/120 mg, 120/80 mg, and 160/40 mg respectively. A solution of PAA in DMF (1.5 mL) was added to a suspension of MOF-5 in DMF (1 mL). The mixture was set to stir at room temperature until complete gelation was observed. Solvent was decanted and the solid was washed with DMF and pressed into a disk at low pressure with a Carver 3851-0 hydraulic press.

Static synthesis. A solution of PAA in DMF (50 mg/mL) was added to a vial containing a slurry of MOF-5 or ZIF-8 in minimal DMF (500 mg/mL). The mixture was briefly shaken on a Scientific Instruments Vortex-Genie 2, allowed to settle, and left to sit at room temperature for two days. A polymer-MOF disk formed at the bottom of the vial, which was flipped and left to sit for an additional two days before removing the disk from solution to dry. The concentration of the remaining polymer solution was determined by UV/Vis absorption and used to calculate MOF loadings. The remaining solution was diluted to 25 mL, and a 0.250 mL aliquot of the dilute solution was further diluted to 50 mL. The absorbance at 300 nm was measured and compared to a calibration curve.

Layered-MOF static synthesis. A solution of PAA (100 mg) in DMF (1 mL) was added to a 2-dram vial containing MOF-5 (100 mg) in minimal DMF (0.2 mL). The mixture was briefly shaken on a vortex and left to sit at room temperature overnight. The polymer-MOF disk was then flipped in the vial and left to sit. After 4 hours, the polymer solution was removed from the vial via pipette and a suspension of ZIF-8 (50 mg) in DMF (0.1 mL) was added onto the surface of the disk. The polymer solution was added back to the vial and left to sit at room temperature overnight. The disk was then removed from the vial and left to dry in air before storing in a desiccator.

Monolith synthesis. MOF-5 or ZIF-8 was added to fill 1.5 mL of a 2-mL vial. A concentrated solution of PAA (200 mg/mL) was added to fill the void space and the vial was briefly shaken on a Scientific Instruments Vortex-Genie 2 until the materials were evenly mixed. The mixture was left to sit overnight at room temperature. The solution was decanted and the vial was broken to extract the polymer-MOF monolith, which was washed with DMF and dried.

PVBA composite synthesis. A solution of PVBA in DMF (100 mg/mL) was added to a vial containing a slurry of MOF-5 or ZIF-8 in minimal DMF (500 mg/mL). The mixture was briefly shaken on a Scientific Instruments Vortex-Genie 2, allowed to settle, and left to sit at room temperature. A solid disk formed, but broke apart upon handling and could not be flipped.

MEPA control experiments. A solution of MEPA (50 mg) in DMF (1 mL) was added to two vials containing slurries of

MOF-5 (50 mg) and ZIF-8 (50 mg), respectively, in minimal DMF (500 mg/mL). The mixtures were briefly shaken on a Scientific Instruments Vortex-Genie 2, allowed to settle, and left to sit at room temperature. After two weeks, a solid composite had not formed and MOF was still readily dispersed with shaking.

UiO-66 control experiments. A solution of PAA in DMF (100 mg/mL) was added to a vial containing a slurry of UiO-66 in DMF (500 mg/mL). The mixture was briefly shaken on a Scientific Instruments Vortex-Genie 2, allowed to settle, and left to sit at room temperature. After two weeks, a solid composite had not formed and MOF was still readily dispersed with shaking.

Thermal treatment. Imidization of materials was achieved using a stepwise thermal sequence modified from the literature.³⁵ The poly(amic acid) or poly(amic acid) hybrid was heated under vacuum at 100°C, 200°C, and 300°C consecutively for one hour each. The material was allowed to cool to room temperature and stored in a desiccator until further use.

Rate study experiments. Polymer-MOF composites were prepared using the static procedure at various concentrations of PAA and MOF-5 in either microcrystalline or nanocrystalline form. To measure concentration during a reaction, a 0.1 mL aliquot of solution was removed and diluted to 10 mL with DMF. A 0.5 or 1.0 mL aliquot of the dilute solution was further diluted to 10 mL with DMF and UV-Vis absorbance of the new dilute solution was measured.

Stability experiments. The materials to be analyzed were removed from the desiccator at one time and left to sit in a fume hood, unsealed and exposed to atmospheric conditions. Structural degradation of MOFs and their composites was monitored using periodic PXRD measurements.

Characterization. ¹H NMR spectra were acquired using a Varian INOVA 400 or 500 MHz spectrometer. Chemical shifts (δ) are reported in parts per million (ppm) referenced using the residual protio solvent peaks as internal standards. Multiplicities are indicated as singlets (*s*) or broad couplings (*br*). UV-Vis absorption was measured using a Cary 8454 UV-Vis Diode Array System with a 10 mm rectangular quartz cuvette. Fourier transform infrared (FT-IR) spectra were acquired with a Perkin Elmer 1760 FT-IR spectrometer with horizontal attenuated total reflectance (HATR). Gel permeation chromatography (GPC) was performed using two Agilent PolyPore 250x6.0 mm columns at 55°C, a Waters 515 HPLC Pump and Waters In-Line Degasser AF, and a Viscotek VE3580 RI detector. The mobile phase was 99.5% N,N-dimethylformamide for HPLC (Acros Organics) with 0.01 M LiBr. Powder X-ray diffraction (PXRD) patterns were collected from a Rigaku Ultima IV system equipped with a Cu source (0.15418 nm $K\alpha$) and operated at 1.76 kW power (40 kV, 44 mA). Diffraction patterns were measured over a range of 5 to 35° 2 θ at a scan rate of 2°/min

Thermogravimetric analysis (TGA) was performed on a TA Instruments DSC SDT Q600 at a heating rate of 10°C/min from 30-900°C under constant N₂ flow (100 mL/min). Glass transition (T_g) temperatures were determined by differential scanning calorimetry (DSC) using a TA Instruments DSCI Q200. Samples were scanned under argon flow (50 mL/min) in three cycles over a range of 40-500°C at a heating rate of 10°C/min. Focused ion beam scanning electron microscope (FIB-SEM) images were captured using a Carl Zeiss AURIGA CrossBeam FIB-

SEM. Samples were gold-coated for 120 seconds using an SPI Module sputter coater and scanned at a 2 keV accelerating voltage. N₂ adsorption measurements were obtained using a Micromeritics Tri-Star II surface area and porosity analyzer at 77K over a relative pressure range of 0.001-0.95 p/p₀. Before analysis, samples were degassed overnight at 150°C on a Micromeritics VacPrep 061 sample degas system. BET surface area was calculated following the Roqueron criteria and IUPAC guidelines.

RESULTS AND DISCUSSION

Component selection and synthesis. For a strategic investigation of post-synthetic exchange hybridization, we selected three of the most well studied MOFs in the literature, MOF-5, ZIF-8, and UiO-66, based on their structural components, physical properties, and facile, cost effective synthetic methods. MOF-5 consists of Zn₄O tetrahedral clusters linked through BDC ligands in a cubic structure with 15.1 Å and 11.0 Å pore volume diameters and an 8.0 Å pore aperture diameter (Figure 4a).^{30,41}

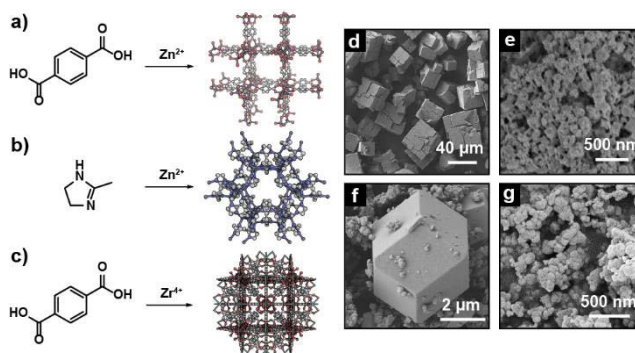
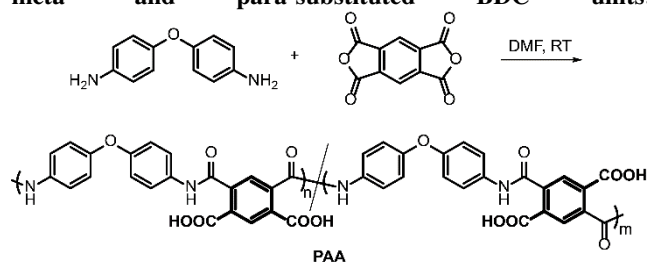


Figure 4. Structural compositions of (a) MOF-5 (CCDC no. 256965), (b) ZIF-8 (CCDC no. 602542), and (c) UiO-66 (CCDC no. 733458). SEM images of (d) microcrystalline MOF-5, (e) nanocrystalline MOF-5, (f) ZIF-8, and (g) UiO-66.

For comparison, ZIF-8 also contains Zn²⁺ ions, but uses 2-MIM linkers to achieve a sodalite topology with 11.6 Å pore diameter and a 3.4 Å pore aperture diameter (Figure 4b).^{33,42} UiO-66 contains the same BDC linker as MOF-5, but connected to 12-coordinate Zr₆O₄(OH)₄ clusters in a face-centered cubic packing arrangement, with 7.5 Å and 12 Å pore diameters and a 6.0 Å pore aperture (Figure 4c).⁴³⁻⁴⁴

Following previously reported procedures, each of the three MOFs was obtained in a nanocrystalline form as identified through scanning electron microscopy (SEM) images (Figure 4e-g), and the structures were confirmed using powder X-ray diffraction (PXRD, Figures S1, S2, S3). MOF-5 was also synthesized in a microcrystalline form (Figure 4d). Slight variations were observed in the diffractogram peak intensities of MOF-5 nanocrystals and microcrystals due to the presence of small zinc impurities throughout the pore volume, which is a common effect of the direct mixing synthetic strategy and does not affect the bulk framework structure.⁴⁵⁻⁴⁸

Scheme 1. Synthesis of PAA as a copolymer containing both meta- and para-substituted BDC units.



Poly(amic acid) (**PAA**) was synthesized via simple step-growth polycondensation of equimolar amounts of pyromellitic dianhydride and 4,4'-oxydianiline (**Scheme 1**). Based on GPC analysis, the resulting polymer had a molecular weight $M_n = 239.5$ kDa (relative to PEO standard) and dispersity $M_w/M_n = 2.09$. (Figure S7, Table S1). A near 1:1 ratio of *meta* and *para* substituted BDC units was revealed by integration of ^1H NMR peaks at 8.31 ppm (*meta* substitution), 7.97 ppm (*para* substitution) and 7.70 ppm (*meta* substitution) (Figure S4). Although the *para* substituted BDC unit is of particular interest as a MOF ligand, it should be noted that the *meta* substituted BDC moiety is also a common coordinating ligand and may be of interest as well. The broad distribution of molecular weight is an effect of the step-growth kinetics, as expected. More importantly, the high molecular weight of the polymer demonstrates that this polymerization effectively reaches very high conversions, allowing for control of molecular weight through monofunctionalized additives. Consequently, addition of aniline during polymerization led to the synthesis of **PAA** with a low molecular weight $M_n = 4.6$ kDa (relative to PEO standard) and dispersity $M_w/M_n = 1.63$ (Figure S7, Table S1). Overall, the component materials for this hybridization method can be obtained through facile synthetic methods using inexpensive starting materials for efficient manufacturing.

Synthesis of polymer-MOF hybrid composites. Though the ideal procedure for ligand exchange involves elevated temperatures, the reaction conditions for this system are limited by the chemical properties of **PAA**. When heated, the polymer begins to imidize in solution, which not only further decreases its low solubility, but also eliminates the BDC groups needed for interaction with MOF crystals. Therefore, all of the polymer-MOF hybrid materials were prepared in DMF at room temperature.

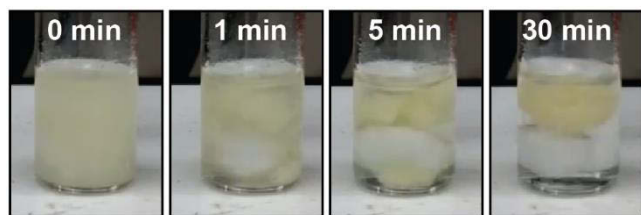


Figure 5. Progressive images of stirred composite formation. Various phases of aggregation are visible, as well as loss of yellow color in the solution.

By stirring a suspension of free MOF in the **PAA**/DMF solution, a single solid composite material formed (referred to as the “stirred” composite). The original solution was yellowish and turbid, the color coming from the dissolved polymer, while turbidity originating from the dispersed MOF crystals. As the solid composite formed, the solution changed from turbid yellow to

clear and colorless, suggesting that both polymer chains and MOF crystals were being integrated into the structure (Figure 5). Separate composites were synthesized using **PAA** with either high or low molecular weights. Under static conditions, the MOF crystals were allowed to settle, and a composite (referred to as the “static” composite) formed in the shape of the bottom of the reaction vessel, e.g. a circular disk at the bottom of a vial. Similarly, a monolith composite can be formed in any shape by filling a mold with MOF powder and saturating the void space with polymer solution. These static methods grant more reproducible control over the shape of the synthesized composites, but require more time for full hybridization. Though stirred composites are fully formed within 24 hours, several days or even weeks may be necessary for maximum polymer incorporation under static conditions. The resulting materials demonstrate the rigid strength of **PAA** as well as low densities relative to the MOF loading percentage, ranging from 5-80%.

Polymer-MOF integration was observed using SEM imaging (Figure 6e-h). The preservation of MOF structural integrity after hybridization was confirmed using PXRD (Figure 6i) and the crystalline facets of particles were clearly visible throughout the composite cross-section, though they were surrounded by the amorphous polymer.

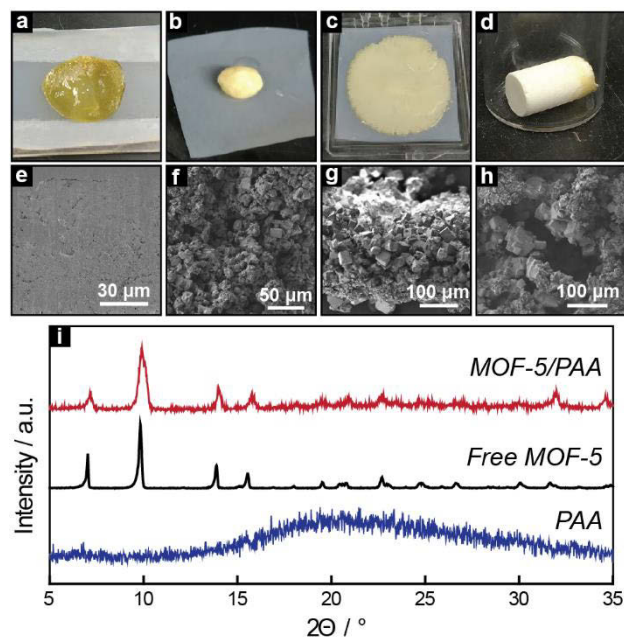


Figure 6. Optical (a-d) and SEM (e-h) images of pure **PAA** (a, e), stirred **MOF-5/PAA** (b, f), static **MOF-5/PAA** (c, g), and **MOF-5/PAA** monolith (d, h). All composites shown are at ~80% MOF loadings. i) PXRD diffractogram of pure **PAA** (blue), free **MOF-5** (black), and **MOF-5/PAA** (red).

Because the polymer is soluble in DMF, the presence of polymer chains in the composite material necessarily implies structural interaction between the chains and MOF particles. SEM analysis revealed the presence of polymer coating on individual crystals that had been removed from solution and washed with DMF before a solid composite had formed (Figure S8). Therefore, we propose a mechanism for this hybridization method wherein the first step involves ligand exchange between individual MOF crystals and free polymer chains (Figure 7).

As the BDC units of **PAA** exchange with the unfunctionalized MOF ligands, each crystal surface quickly becomes coated with polymer chains. Once tethered, a polymer chain will then undergo ligand exchange at a second coordination site. As single polymers begin coordinating to multiple crystals, the result is a crosslinked network of MOFs connected through a **PAA** matrix. In contrast to mixed matrix membrane synthesis through solution film casting and solvent evaporation, this method allows for a controlled dispersion of MOF throughout the composite.

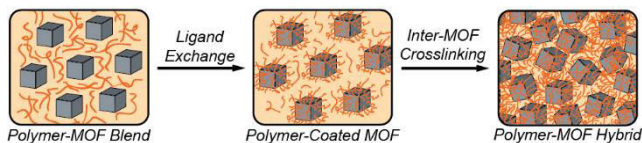


Figure 7. Cartoon of proposed mechanism for hybridization through ligand exchange between MOF crystals and polymer chains.

Mechanistic studies. To confirm that the polymer-MOF interactions are coordination-based rather than physisorption, a control polymer, poly(dicarbomethoxyterephthalic acid-*co*-4,4'-oxydianiline) (referred to as “methyl ester polyamide or **MEPA**) was used for the hybridization procedure instead of **PAA**. The structure of **MEPA** is similar to that of **PAA**, but is methylated to block coordination at the carboxylate sites (Figure 8, ^1H NMR spectrum in Figure S5). When left to sit or stir for over two weeks with each of the three MOFs, in no case was there sufficient interaction between the polymer and MOF to form a solid composite. The size and rigidity of the polymer chains likely prevents them from fitting inside the MOF pores so neither surface exchange nor host-guest interactions are possible.

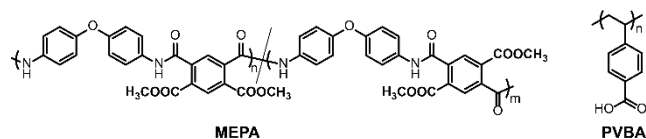


Figure 8. Structures of **MEPA**, with methyl ester functionalizations to block coordination at the dicarboxylates, and **PVBA**, with a single benzene carboxylate at each repeat unit.

Poly(4-vinylbenzoic acid) (**PVBA**) was used as a control polymer with a benzene carboxylate coordination site at each repeat unit, but without the dicarboxylate functionality (Figure 8, ^1H NMR spectrum in Figure S6). Using suspensions of MOF-5 in a **PVBA**/DMF solution, a composite material was obtained. The solid was very fragile compared to the **PAA** composites, likely due to the weaker physical properties of the polymer itself as well as weaker polymer-MOF interactions because the monocarboxylate cannot fully replace the parent dicarboxylates, only binding through one site. Monofunctionalized ligand substitution has been shown to cause structural defects and disorder in MOFs⁴⁹⁻⁵⁰, which likely weakens the crystal structure significantly and limits the mechanical properties of the composite. Nonetheless, the successful hybridization of both **PAA** and **PVBA** along with the failed hybridization of **MEPA** supports a coordination-based ligand exchange mechanism. Moreover, the coordination of **PVBA** to MOF crystals suggests that both *para* and *meta* substituted BDC units in **PAA** may contribute to polymer-MOF integration, rather than only *para* substituted units.

The structures of MOF-5, ZIF-8, and UiO-66 are particularly useful for investigating the effects of different coordination environments on polymer-MOF hybridization. The remarkable water stability of UiO-66 is attributed to the higher oxidation state of Zr^{4+} and the inert Zr-carboxylate bonds,⁵¹⁻⁵² in contrast to the more labile Zn-carboxylate or Zn-imidazolite bonds.^{46, 53-54} Consequently, the postsynthetic ligand exchange studies performed by Cohen et. al. demonstrate low exchange percentages for UiO-66 particles suspended in free ligand solution for 5 days at room temperature.²⁸ Higher exchange percentages were reported at elevated temperatures; however, the temperature for exchange with **PAA** must be kept at room temperature to prevent imidization (while the onset temperature for imidization in the solid state is around 150°C, in solution and in the presence of additives it can occur at much lower temperatures⁵⁵). Additionally, the rate of exchange between **PAA** and UiO-66 is likely even lower due to limited mobility of the polymer chains relative to free small-molecule ligands. Successful crosslinking of MOFs not only requires close proximity of particles, but correct orientation of polymer chains to reach more than one particle at once. If the rate of exchange is lower than the rate of diffusion, it is unlikely that hybridization through crosslinking will occur.

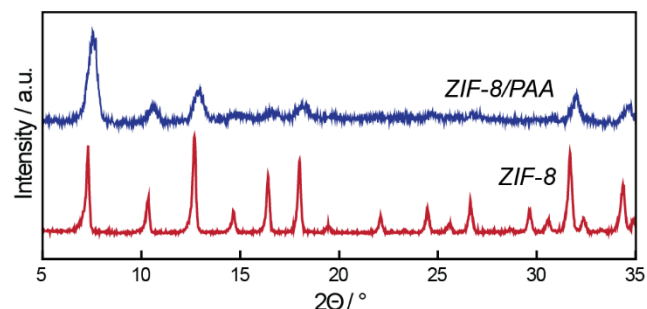


Figure 9. PXRD diffractograms of ZIF-8 (bottom) and ZIF-8/PAA (top).

Probing further, ZIF-8 was used to study the importance of MOF geometry for ligand substitution. ZIF-8 contains Zn^{2+} ions at its nodes similarly to MOF-5, but the nodes are closer together due to the smaller size and coordination angle of the 2-MIM ligand compared to BDC. Despite this geometry difference however, **ZIF-8/PAA** composites were successfully synthesized with the ZIF-8 structure intact as confirmed by PXRD (Figure 9). On the other hand, UiO-66, which contains BDC ligands connected by zirconium-based nodes, did not form a composite under any conditions.

These findings align with known behaviors of MOF ligand exchange. It is unlikely that a BDC ligand would exchange perfectly with 2-MIM; however, it is possible for a carboxylate to exchange and coordinate partially at the MOF surface, tethering polymer chains through surface modifications similar to those observed using monofunctionalized ligands.⁵⁶ Therefore, **MOF-5/PAA** and **ZIF-8/PAA** hybridizations yield similar composites because they both involve BDC/ Zn^{2+} coordination and similar exchange rates. These ligand exchange trends not only further support the hypothesis that the hybrid materials form through a postsynthetic exchange mechanism, but also demonstrate that the method is applicable to a wide range of framework types.

Due to the heterogeneous and dynamic nature of the ligand exchange method, the hybridization process allows for continued modification beyond initial fabrication. Even after a composite is fully formed and saturated with polymer, it is possible to add additional MOF particles to continue crosslinking, forming MOF-dense and polymer-dense layers. As a proof-of-concept experiment, a **MOF-5/PAA** static disk was formed using the typical method. After sitting in solution for one day, ZIF-8 particles were added to the vial and allowed to settle on top of the disk. As expected, ZIF-8 tethered to **PAA** on the disk surface as new polymer chains were incorporated from solution to form a **MOF-5/ZIF-8** bilayer composite with PAA (Figure 10).

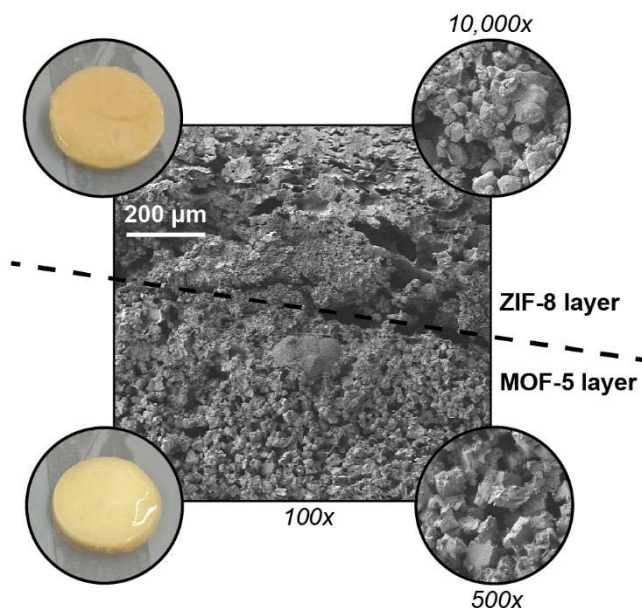


Figure 10. SEM image of **MOF-5/ZIF-8** bilayer composite with PAA at 100x magnification, with insets showing optical images and increased magnification at each layer.

To further investigate the hybridization behavior, rate studies were performed using varying polymer and MOF initial concentrations. Rates were observed by monitoring the concentration of residual **PAA** in DMF solution throughout static composite formation using UV-Vis absorption spectroscopy. As shown in Figure 11, a clear increase in reaction rate was observed when the concentration of MOF was increased at constant **PAA** concentration. When keeping MOF concentration constant and varying **PAA** concentration, no significant change in rate was observed. Additionally, the timescales of the syntheses should be noted, as different sizes of MOF-5 crystals were used. When microcrystalline MOF-5 was used, the reaction reached equilibrium in no less than 16 days at the highest MOF concentration. Using nanocrystalline MOF-5 however, equilibrium was achieved within two to three days.

Given that the smaller crystals have a much higher external surface area, these combined results suggest that the rate is not necessarily dependent on the number of MOF crystals explicitly, but rather the total number of exchangeable ligand sites. Furthermore, the rate is not dependent on polymer concentration, therefore implying that the slow step in polymer integration is dissociation of the original MOF ligands, with polymer coordination happening readily.

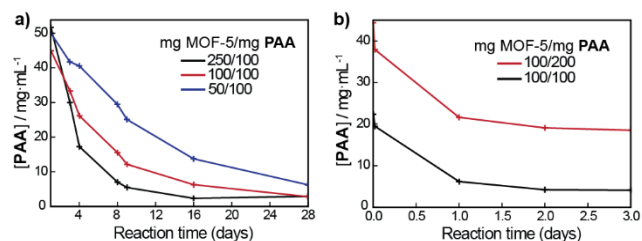


Figure 11. Change in residual **PAA** concentration over time at (a) varying initial microcrystalline MOF-5 concentrations, and (b) varying initial **PAA** concentrations using nanocrystalline MOF-5.

Through these concentration experiments, it was also observed that some of the reactions approach similar final **PAA** concentrations of 5 mg/mL or less, yet others equilibrate at higher **PAA** concentrations. It seems that a lower limit for MOF loadings in the static composite materials exists between approximately 40-50%. If the initial amount of MOF-5 is above this percent range, then almost all of the polymer will eventually become integrated. Below a 40% initial MOF loading, we expect that there are too many polymer chains for the available coordination sites and the reaction equilibrates when the maximum number of chains has been incorporated. For decreased loadings, the use of stirring further breaks down MOF crystals to increase surface area until all polymer has been incorporated, allowing for synthesis of composites with loadings as low as 10%. Based on these mechanistic properties, we have concluded that the ligand exchange method is not only effective for polymer-MOF hybridization, but that the synthesis is controlled and reproducible. By strategically varying the ratios of MOF, polymer, and solvent, composites can be formed at specific loadings in a desired amount of time.

Thermal imidization. A particularly unique feature of the poly(amic acid) system is the ability to convert the polymer to the polyimide (**PI**) form at any point simply by using a thermal treatment. Such a quality is appealing because it allows for the synthesis of materials with increased strength and stability which would not otherwise be processable due to insolubility.²⁶ Through the soluble poly(amic acid) intermediate, these materials can be cast or molded before carrying out the imidization process. In addition to its inclusion of a BDC moiety, this system is attractive for polymer-MOF hybridization because the solution phase **PAA** can be integrated with MOF crystals in the desired form, then heated to imidize the non-coordinated polymer repeat units, theoretically improving the properties of the composite even further. To imidize the materials, a stepwise curing procedure was used in which samples were heated under vacuum at 100°C, 200°C, and 300°C for one hour each. Conversion of **MOF-5/PAA** to **MOF-5/PI** was confirmed using attenuated total reflectance-Fourier transform infrared spectroscopy (ATR-FTIR) (Figure S9, S10). Analysis is made more difficult due to overlap with MOF-5 peaks, but the appearance of peaks at 1775 cm⁻¹ (imide C=O stretch) and 725 cm⁻¹ (imide ring deformation) as well as the loss of peak resolution at 1550 cm⁻¹ (C-NH stretch) clearly identifies the new presence of imide groups. Furthermore, the structural integrity of MOF-5 was evaluated using PXRD after imidization (Figure S1). As expected given the thermal stability of the MOF, no significant changes in the powder pattern were observed, thus confirming the successful synthesis of a **MOF-5/PI** hybrid composite.

Physical properties of hybrid composites. Once synthesized, the polymer-MOF materials were analyzed for improvements in bulk physical properties compared to the original components. Thermogravimetric analyses (TGA) showed no significant changes in thermal stability after hybridization, with features of both the polymer and MOF components present in the thermal curves for each composite (Figure S11, S12, S13). Likewise, differential scanning calorimetry (DSC) curves did not show significant changes in polymer T_g after MOF incorporation (Figure S14).

To measure the ambient stability of the composites, samples were exposed to atmospheric humidity for an extended period of time and structural changes were monitored using PXRD (Figure 12a). Zeolitic frameworks such as ZIF-8 are known for their robust stability in humid air due to the Zn-N bond strength.⁴² MOF-5, however, is greatly limited by hydrolytic instability and can show signs of structural degradation within minutes of exposure to atmospheric moisture.⁵⁷

Within a full day of exposure, we observed total irreversible degradation in pure microcrystalline MOF-5, as indicated primarily by the characteristic disappearance of the peak at $2\theta=6.8^\circ$ and the shift of a major peak from $2\theta=9.6^\circ$ to $2\theta=9.0^\circ$. When integrated into a polymer hybrid at a MOF loading of approximately 80%, MOF-5 structural stability increased remarkably, with no appearance of degradation peaks for up to at least 20 days.

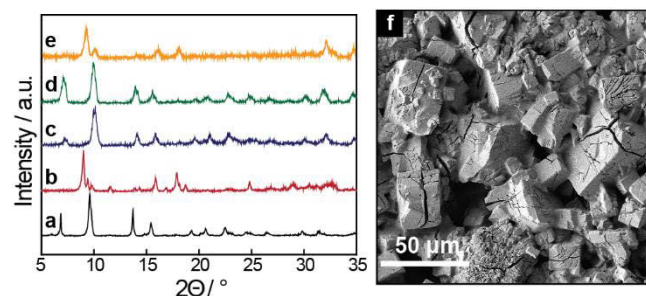


Figure 12. PXRD diffractograms of (a) fresh MOF-5, (b) MOF-5 exposed to humid air for 2 days, (c) MOF-5/PAA exposed to humid air for 20 days, (d) MOF-5/PI exposed to humid air for 12 days, (e) MOF-5/PI exposed to humid air for 20 days, and (f) SEM image of MOF-5/PI surface showing cracks in crystals.

Interestingly, the imidized samples consistently demonstrated lower stability than those which were not imidized, with degradation occurring between 12 and 20 days. Although this result is unexpected based solely on the increased rigidity and hydrophobicity of the polyimide chains, SEM images of the imidized samples reveal large cracks throughout the material. It is thus possible that as the chains imidized and become locked into new conformations, they physically pull on the crystals to which they are tethered, forming cracks which allow exposure of MOF-5 to moisture (Figure 12b). The materials were also tested for stability when fully submerged in water; however, full degradation was observed within a day under such high exposure.

Arguably one of their more important physical properties, porosity contributes significantly to the functionality of metal-organic frameworks. A major disadvantage to many methods of MOF hybridization is the pore-filling effect from introducing new large molecules into the free volume, decreasing the amount of space available for host-guest interactions.¹⁷ To test

whether or not the MOF pore structures are affected by PAA integration, N_2 adsorption experiments were used to measure the surface areas of pure MOFs and their respective hybrid composites (Figure 13, S15, S16). The BET surface area of microcrystalline MOF-5 powder was calculated to be $588 \text{ m}^2\text{g}^{-1}$, consistent with the direct mixing synthetic route.⁴⁵ For a microcrystalline MOF-5/PAA disk at 77% MOF loading, a BET surface area of $452 \text{ m}^2\text{g}^{-1}$ was measured. When weight fraction of MOF within a composite is taken into account, the MOF surface area normalizes to $587 \text{ m}^2\text{g}^{-1}$, suggesting a 99.8% retention of porosity during hybridization. This level of porosity preservation is unprecedented, and is likely due to the large size of PAA chains, which prevents them from entering MOF pores and limits ligand exchange to the crystal surface.

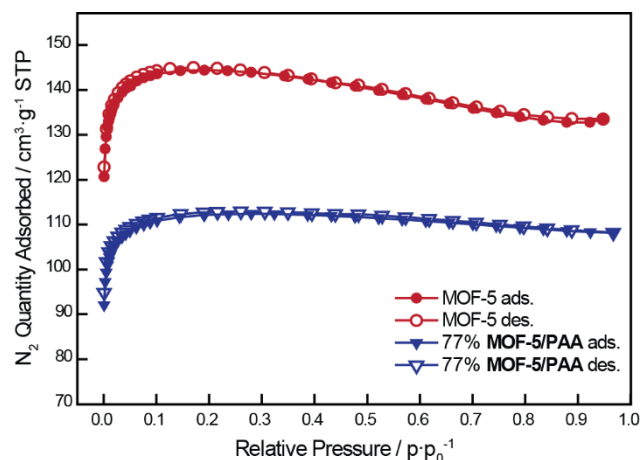


Figure 13. N_2 adsorption-desorption isotherms of microcrystalline MOF-5 (top) and MOF-5/PAA composites (bottom) at 77% MOF loading.

More significant decreases in surface areas were observed in composites using nanocrystalline MOFs. The BET surface area of pure ZIF-8 was calculated to be $1016 \text{ m}^2\text{g}^{-1}$, while the BET surface area of a ZIF-8/PAA composite at 69% MOF loading was calculated to be $435 \text{ m}^2\text{g}^{-1}$, or $630 \text{ m}^2\text{g}^{-1}$ normalized for ZIF-8. For nanocrystalline MOF-5, a decrease in BET surface was observed from $1119 \text{ m}^2\text{g}^{-1}$ for the pure MOF to $51 \text{ m}^2\text{g}^{-1}$, or $102 \text{ m}^2\text{g}^{-1}$ normalized, for a composite material at 50% loading. Given that the ZIF-8 crystals are smaller than microcrystalline MOF-5 by at least an order of magnitude, and the nanocrystalline MOF-5 crystals are smaller than ZIF-8 by at least an order of magnitude, these decreases in surface area suggest that the available porosity of these polymer-MOF composites is influenced by the size of the MOF crystals. Even with surface-limited interactions, the loss of any porosity near the crystal surface may become more relevant at nanometer scales. Additionally, SEM images of composites formed under static conditions from nanocrystalline MOF-5 reveal smooth spherical features throughout the material (Figure 14a). Cross-section images show that these features are actually pod-like structures containing clusters of MOF crystals surrounded by a polymer-dense coating which likely blocks external access to the MOF pore volume (Figure 14b). These findings demonstrate the importance of MOF crystal size for designing high porosity hybrid composites, while further investigations are necessary to elucidate the role of MOF size in the material morphology and to optimize the available surface area.

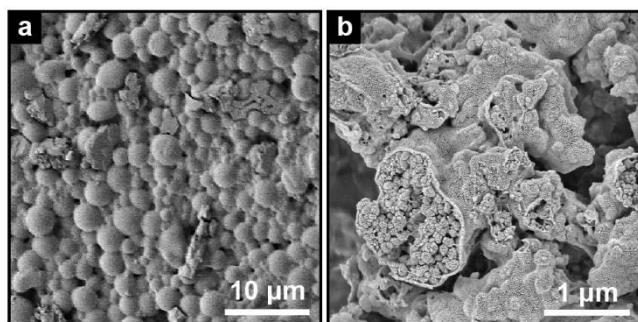


Figure 14. SEM images of nanocrystalline MOF-5/PAA composite at 50% MOF loading. (a) surface image showing spherical features, and (b) cross-section showing pod-like structures of MOF crystals surrounded by polymer-dense coating.

CONCLUSIONS

Hybrid PAA-MOF composites have been synthesized at MOF loadings as high as 80% using postsynthetic ligand exchange methods to incorporate polymer chains into framework structures. Synthesis has been achieved using both microcrystalline and nanocrystalline MOF-5 as well as ZIF-8, though composites incorporating UiO-66 failed to synthesize due to the lower exchange rates of the zirconium nodes. The reaction is independent of concentration of polymers, while the rate is highly dependent on the number of exchangeable ligand sites at MOF surfaces, controlled by particle size and concentration. These novel materials have demonstrated nearly full preservation of MOF porosity, as well as hydrolytic stability for at least twenty days. This versatile method for the fabrication of monolithic polymer-MOF composite opens new avenues for the further development of a vast library of functional hybrid materials.

ASSOCIATED CONTENT

Supporting Information. Video of composite formation; PXRD diffractograms of MOFs and composites; polymer ^1H NMR spectra, GPC traces, and molecular weight data; SEM images of polymer-coated MOF; FT-IR spectra of polymer and composites before and after imidization.

AUTHOR INFORMATION

Corresponding Author

E-mail: jrzayev@buffalo.edu

E-mail: trcook@buffalo.edu

ORCID

Vincent J. Pastore: 0000-0002-0666-5885

Timothy R. Cook: 0000-0002-7668-8089

Javid Rzaev: 0000-0002-9280-1811

Notes

The authors declare no competing financial interest.

ACKNOWLEDGMENT

We would like to thank University at Buffalo and the National Science Foundation (DMR-1709371) for financial support.

REFERENCES

(1) Farha, O. K.; Hupp, J. T., Rational Design, Synthesis, Purification, and Activation of Metal–Organic Framework Materials. *Acc. Chem. Res.* **2010**, *43*, 1166-1175.

(2) Férey, G., Hybrid porous solids: past, present, future. *Chem. Soc. Rev.* **2008**, *37*, 191-214.

(3) Cook, T. R.; Zheng, Y.-R.; Stang, P. J., Metal–Organic Frameworks and Self-Assembled Supramolecular Coordination Complexes: Comparing and Contrasting the Design, Synthesis, and Functionality of Metal–Organic Materials. *Chem. Rev.* **2013**, *113*, 734-777.

(4) Furukawa, H.; Cordova, K. E.; O’Keeffe, M.; Yaghi, O. M., The Chemistry and Applications of Metal–Organic Frameworks. *Science* **2013**, *341*, 1230444-1-1230444-12.

(5) Horcajada, P.; Gref, R.; Baati, T.; Allan, P. K.; Maurin, G.; Couvreur, P.; Férey, G.; Morris, R. E.; Serre, C., Metal–Organic Frameworks in Biomedicine. *Chem. Rev.* **2012**, *112*, 1232-1268.

(6) Kreno, L. E.; Leong, K.; Farha, O. K.; Allendorf, M.; Van Duyne, R. P.; Hupp, J. T., Metal–Organic Framework Materials as Chemical Sensors. *Chem. Rev.* **2012**, *112*, 1105-1125.

(7) Li, J.-R.; Kuppler, R. J.; Zhou, H.-C., Selective gas adsorption and separation in metal-organic frameworks. *Chem. Soc. Rev.* **2009**, *38*, 1477-1504.

(8) Sumida, K.; Rogow, D. L.; Mason, J. A.; McDonald, T. M.; Bloch, E. D.; Herm, Z. R.; Bae, T.-H.; Long, J. R., Carbon Dioxide Capture in Metal–Organic Frameworks. *Chem. Rev.* **2012**, *112*, 724-781.

(9) Susumu, K.; Ryo, K.; Shin-ichiro, N., Functional Porous Coordination Polymers. *Angew. Chem., Int. Ed.* **2004**, *43*, 2334-2375.

(10) Talin, A. A.; Centrone, A.; Ford, A. C.; Foster, M. E.; Stavila, V.; Haney, P.; Kinney, R. A.; Szalai, V.; El Gabaly, F.; Yoon, H. P.; Léonard, F.; Allendorf, M. D., Tunable Electrical Conductivity in Metal-Organic Framework Thin-Film Devices. *Science* **2014**, *343*, 66-69.

(11) Gamage, N. D. H.; McDonald, K. A.; Matzger, A. J., MOF-5-Polystyrene: Direct Production from Monomer, Improved Hydrolytic Stability, and Unique Guest Adsorption. *Angew. Chem., Int. Ed.* **2016**, *55*, 12099-12103.

(12) Feng, P. L.; Perry, J. J.; Nikodemski, S.; Jacobs, B. W.; Meek, S. T.; Allendorf, M. D., Assessing the Purity of Metal–Organic Frameworks Using Photoluminescence: MOF-5, ZnO Quantum Dots, and Framework Decomposition. *J. Am. Chem. Soc.* **2010**, *132*, 15487-15489.

(13) Rodriguez, N. A.; Parra, R.; Grela, M. A., Structural characterization, optical properties and photocatalytic activity of MOF-5 and its hydrolysis products: implications on their excitation mechanism. *RSC Adv.* **2015**, *5*, 73112-73118.

(14) Todaro, M.; Buscarino, G.; Sciortino, L.; Alessi, A.; Messina, F.; Taddei, M.; Ranocchiaro, M.; Cannas, M.; Gelardi, F. M., Decomposition Process of Carboxylate MOF HKUST-1 Unveiled at the Atomic Scale Level. *J. Phys. Chem. C* **2016**, *120*, 12879-12889.

(15) Kitao, T.; Zhang, Y.; Kitagawa, S.; Wang, B.; Uemura, T., Hybridization of MOFs and polymers. *Chem. Soc. Rev.* **2017**, *46*, 3108-3133.

(16) Zhang, Y.; Feng, X.; Li, H.; Chen, Y.; Zhao, J.; Wang, S.; Wang, L.; Wang, B., Photoinduced Postsynthetic Polymerization of a Metal–Organic Framework toward a Flexible Stand-Alone Membrane. *Angew. Chem.* **2015**, *127*, 4333-4337.

(17) McDonald, K. A.; Feldblyum, J. I.; Koh, K.; Wong-Foy, A. G.; Matzger, A. J., Polymer@MOF@MOF: "grafting from" atom transfer radical polymerization for the synthesis of hybrid porous solids. *Chem. Commun.* **2015**, *51*, 11994-11996.

(18) Nagata, S.; Kokado, K.; Sada, K., Metal-organic framework tethering PNIPAM for ON-OFF controlled release in solution. *Chem. Commun.* **2015**, *51*, 8614-8617.

(19) Zimpel, A.; Preiß, T.; Röder, R.; Engelke, H.; Ingrisch, M.; Peller, M.; Rädler, J. O.; Wagner, E.; Bein, T.; Lächelt, U.; Wuttke, S., Imparting Functionality to MOF Nanoparticles by External Surface Selective Covalent Attachment of Polymers. *Chem. Mater.* **2016**, *28*, 3318-3326.

(20) Zhang, Z.; Nguyen, H. T. H.; Miller, S. A.; Cohen, S. M., polyMOFs: A Class of Interconvertible Polymer-Metal-Organic-

- Framework Hybrid Materials. *Angew. Chem., Int. Ed.* **2015**, *54*, 6152-6157.
- (21) MacLeod, M. J.; Johnson, J. A., Block co-polyMOFs: assembly of polymer-polyMOF hybrids via iterative exponential growth and "click" chemistry. *Polym. Chem.* **2017**, *8*, 4488-4493.
- (22) Perez, E. V.; Balkus, K. J.; Ferraris, J. P.; Musselman, I. H., Mixed-matrix membranes containing MOF-5 for gas separations. *J. Membr. Sci.* **2009**, *328*, 165-173.
- (23) Ren, H.; Jin, J.; Hu, J.; Liu, H., Affinity between Metal–Organic Frameworks and Polyimides in Asymmetric Mixed Matrix Membranes for Gas Separations. *Ind. Eng. Chem. Res.* **2012**, *51*, 10156-10164.
- (24) Xiao, Y.; Low, B. T.; Hosseini, S. S.; Chung, T. S.; Paul, D. R., The strategies of molecular architecture and modification of polyimide-based membranes for CO₂ removal from natural gas—A review. *Prog. Polym. Sci.* **2009**, *34*, 561-580.
- (25) Sroog, C. E.; Endrey, A. L.; Abramo, S. V.; Berr, C. E.; Edwards, W. M.; Olivier, K. L., Aromatic polypyromellitimides from aromatic polyamic acids. *J. Polym. Sci., Part A: Polym. Chem.* **1965**, *3*, 1373-1390.
- (26) Hsiao, S.-H.; Chen, Y.-J., Structure–property study of polyimides derived from PMDA and BPDA dianhydrides with structurally different diamines. *Eur. Polym. J.* **2002**, *38*, 815-828.
- (27) Gross, A. F.; Sherman, E.; Mahoney, S. L.; Vajo, J. J., Reversible Ligand Exchange in a Metal–Organic Framework (MOF): Toward MOF-Based Dynamic Combinatorial Chemical Systems. *J. Phys. Chem. A* **2013**, *117*, 3771-3776.
- (28) Kim, M.; Cahill, J. F.; Su, Y.; Prather, K. A.; Cohen, S. M., Postsynthetic ligand exchange as a route to functionalization of 'inert' metal-organic frameworks. *Chem. Sci.* **2012**, *3*, 126-130.
- (29) S., D. M.; M., C. S., In Situ Modification of Metal–Organic Frameworks in Mixed-Matrix Membranes. *Angew. Chem., Int. Ed.* **2015**, *54*, 9029-9032.
- (30) Li, H.; Eddaoudi, M.; O'Keeffe, M.; Yaghi, O. M., Design and synthesis of an exceptionally stable and highly porous metal-organic framework. *Nature* **1999**, *402*, 276-279.
- (31) Mueller, U.; Schubert, M.; Teich, F.; Puetter, H.; Schierle-Arndt, K.; Pastre, J., Metal-organic frameworks-prospective industrial applications. *J. Mater. Chem.* **2006**, *16*, 626-636.
- (32) Huang, L.; Wang, H.; Chen, J.; Wang, Z.; Sun, J.; Zhao, D.; Yan, Y., Synthesis, morphology control, and properties of porous metal-organic coordination polymers. *Microporous Mesoporous Mater.* **2003**, *58*, 105-114.
- (33) Lee, Y.-R.; Jang, M.-S.; Cho, H.-Y.; Kwon, H.-J.; Kim, S.; Ahn, W.-S., ZIF-8: A comparison of synthesis methods. *Chem. Eng. J.* **2015**, *271*, 276-280.
- (34) Katz, M. J.; Brown, Z. J.; Colon, Y. J.; Siu, P. W.; Scheidt, K. A.; Snurr, R. Q.; Hupp, J. T.; Farha, O. K., A facile synthesis of UiO-66, UiO-67 and their derivatives. *Chem. Commun.* **2013**, *49*, 9449-9451.
- (35) Ayala, D.; Lozano, A. E.; Abajo, J. D.; Campa, J. G. D. L., Synthesis and characterization of novel polyimides with bulky pendant groups. *J. Polym. Sci., Part A: Polym. Chem.* **1999**, *37*, 805-814.
- (36) Ishii, J.; Takata, A.; Oami, Y.; Yokota, R.; Vladimirov, L.; Hasegawa, M., Spontaneous molecular orientation of polyimides induced by thermal imidization (6). Mechanism of negative in-plane CTE generation in non-stretched polyimide films. *Eur. Polym. J.* **2010**, *46*, 681-693.
- (37) Park, S. K.; Park, S. Y.; Lee, C. J., Direct polymerization of aromatic diacid dimethyl esters with aromatic diamines II. Control of copolyimide chemical structure. *Polymer* **2000**, *41*, 433-440.
- (38) Wu, G.-C.; Tanaka, H.; Sanui, K.; Ogata, N., Synthesis of Poly(p-benzamide) with Triphenylphosphine and Hexachloroethane Reagents–Reaction Conditions. *Polym. J.* **1982**, *14*, 571-574.
- (39) Ourdani, S.; Amrani, F., Study of the miscibility of poly(styrene-co-4-vinylbenzoic acid) with poly(ethyl methacrylate) or with poly[ethyl methacrylate-co-(2-N,N-dimethylaminoethyl) methacrylate] by inverse gas chromatography. *J. Chromatogr., A* **2002**, *969*, 287-299.
- (40) Wang, S.; Li, X.; Xun, S.; Wan, X.; Wang, Z. Y., Near-Infrared Electrochromic and Electroluminescent Polymers Containing Pendant Ruthenium Complex Groups. *Macromolecules* **2006**, *39*, 7502-7507.
- (41) Tsao, C.-S.; Yu, M.-S.; Chung, T.-Y.; Wu, H.-C.; Wang, C.-Y.; Chang, K.-S.; Chen, H.-L., Characterization of Pore Structure in Metal–Organic Framework by Small-Angle X-ray Scattering. *J. Am. Chem. Soc.* **2007**, *129*, 15997-16004.
- (42) Park, K. S.; Ni, Z.; Côté, A. P.; Choi, J. Y.; Huang, R.; Uribe-Romo, F. J.; Chae, H. K.; O'Keeffe, M.; Yaghi, O. M., Exceptional chemical and thermal stability of zeolitic imidazolate frameworks. *Proc. Natl. Acad. Sci.* **2006**, *103*, 10186-10191.
- (43) Cavka, J. H.; Jakobsen, S.; Olsbye, U.; Guillou, N.; Lamberti, C.; Bordiga, S.; Lillerud, K. P., A New Zirconium Inorganic Building Brick Forming Metal Organic Frameworks with Exceptional Stability. *J. Am. Chem. Soc.* **2008**, *130*, 13850-13851.
- (44) Peterson, G. W.; Moon, S.-Y.; Wagner, G. W.; Hall, M. G.; DeCoste, J. B.; Hupp, J. T.; Farha, O. K., Tailoring the Pore Size and Functionality of UiO-Type Metal–Organic Frameworks for Optimal Nerve Agent Destruction. *Inorg. Chem.* **2015**, *54*, 9684-9686.
- (45) Hafizovic, J.; Bjørgen, M.; Olsbye, U.; Dietzel, P. D. C.; Bordiga, S.; Prestipino, C.; Lamberti, C.; Lillerud, K. P., The Inconsistency in Adsorption Properties and Powder XRD Data of MOF-5 Is Rationalized by Framework Interpenetration and the Presence of Organic and Inorganic Species in the Nanocavities. *J. Am. Chem. Soc.* **2007**, *129*, 3612-3620.
- (46) Kaye, S. S.; Dailly, A.; Yaghi, O. M.; Long, J. R., Impact of Preparation and Handling on the Hydrogen Storage Properties of Zn₄O(1,4-benzenedicarboxylate)₃ (MOF-5). *J. Am. Chem. Soc.* **2007**, *129*, 14176-14177.
- (47) Li, J.; Cheng, S.; Zhao, Q.; Long, P.; Dong, J., Synthesis and hydrogen-storage behavior of metal-organic framework MOF-5. *Int. J. Hydrogen Energy.* **2008**, *34*, 1377-1382.
- (48) Tranchemontagne, D. J.; Hunt, J. R.; Yaghi, O. M., Room temperature synthesis of metal-organic frameworks: MOF-5, MOF-74, MOF-177, MOF-199, and IRMOF-0. *Tetrahedron* **2008**, *64*, 8553-8557.
- (49) Cheetham, A. K.; Bennett, T. D.; Coudert, F.-X.; Goodwin, A. L., Defects and disorder in metal organic frameworks. *Dalton Trans.* **2016**, *45*, 4113-4126.
- (50) Shearer, G. C.; Chavan, S.; Bordiga, S.; Svelle, S.; Olsbye, U.; Lillerud, K. P., Defect Engineering: Tuning the Porosity and Composition of the Metal–Organic Framework UiO-66 via Modulated Synthesis. *Chem. Mater.* **2016**, *28*, 3749-3761.
- (51) Kandiah, M.; Nilsen, M. H.; Usseglio, S.; Jakobsen, S.; Olsbye, U.; Tilsted, M.; Larabi, C.; Quadrelli, E. A.; Bonino, F.; Lillerud, K. P., Synthesis and Stability of Tagged UiO-66 Zr-MOFs. *Chem. Mater.* **2010**, *22*, 6632-6640.
- (52) Piscopo, C. G.; Polyzoidis, A.; Schwarzer, M.; Loebecke, S., Stability of UiO-66 under acidic treatment: Opportunities and limitations for post-synthetic modifications. *Microporous Mesoporous Mater.* **2015**, *208*, 30-35.
- (53) Zhang, H.; Liu, D.; Yao, Y.; Zhang, B.; Lin, Y. S., Stability of ZIF-8 membranes and crystalline powders in water at room temperature. *J. Membr. Sci.* **2015**, *485*, 103-111.
- (54) Sheng, L.; Yang, F.; Wang, C.; Yu, J.; Zhang, L.; Pan, Y., Comparison of the hydrothermal stability of ZIF-8 nanocrystals and polycrystalline membranes derived from zinc salt variations. *Mater. Lett.* **2017**, *197*, 184-187.
- (55) Oba, M., Effect of curing accelerators on thermal imidization of polyamic acids at low temperature. *J. Polym. Sci., Part A: Polym. Chem.* **1996**, *34*, 651-658.
- (56) McGuire, C. V.; Forgan, R. S., The surface chemistry of metal-organic frameworks. *Chem. Commun.* **2015**, *51*, 5199-5217.
- (57) Ming, Y.; Purewal, J.; Yang, J.; Xu, C.; Soltis, R.; Warner, J.; Veenstra, M.; Gaab, M.; Müller, U.; Siegel, D. J., Kinetic Stability of MOF-5 in Humid Environments: Impact of Powder Densification, Humidity Level, and Exposure Time. *Langmuir* **2015**, *31*, 4988-4995.

